

The Mu3e Experiment at PSI

Alessandro Bravar
for the Mu3e Collaboration

University of Geneva
alessandro.bravar@unige.ch

November 30, 2018



*Proceedings for the 15th International Workshop on Tau Lepton Physics,
Amsterdam, The Netherlands, 24-28 September 2018*

scipost.org/SciPostPhysProc.Tau2018

1 Abstract

Mu3e will search for charged Lepton Flavor Violation in the neutrinoless muon decay $\mu^+ \rightarrow e^+e^-e^+$ with a sensitivity down to 10^{-16} (90% C.L.) using the world most intense continuous muon beam at PSI. This search requires a large acceptance detector capable of coping with rates of up to 2×10^9 stopped muons per second with excellent momentum, spatial, and time resolution. The Mu3e detector is based on thin monolithic active silicon pixel sensors for tracking in conjunction with scintillating fibers and tiles for timing measurements. The Mu3e apparatus is under constructions and first data is expected in 2020.

10 1 Introduction

In the Standard Model of particle physics lepton flavor is strictly conserved. The discovery of neutrino oscillations, however, has shown that lepton flavor conservation is not a symmetry of Nature, although the observation of flavor violation in the charged lepton sector is still missing. Processes like the $\mu^+ \rightarrow e^+e^-e^+$ or the $\mu^+ \rightarrow e^+\gamma$ decays, or the $\mu^\pm A \rightarrow e^\pm A$ conversion have not yet been observed. In extensions of the Standard Model (SM) with neutrino mixing, lepton flavor violating muon decays can be mediated, for example, by loop diagrams (see Figure 1 left). Loop diagrams involving massive neutrinos, however, are strongly suppressed with branching ratios $\mathcal{O} \sim 10^{-54}$ and thus give potentially high sensitivity to charged Lepton Flavor Violation (cLFV) processes, because of the absence of SM backgrounds. Hence, any observation of cLFV would be a clear sign for new physics beyond the SM at scales far beyond the reach of direct observation, up to several PeV, as illustrated in Figure 2.

Lepton flavor conservation is naturally violated in many extensions of the Standard Model [1]. In several models [2,3] sizable cLFV effects, accessible to the new generation of high sensitivity experiments, are predicted. Several models, such as grand unified theories (GUTs), supersymmetric models (Figure 1 center), compositeness, leptoquarks, left-right symmetric models, seesaw models, etc. predict an experimentally accessible amount of cLFV. cLFV can also be mediated by tree couplings involving new particles (Figure 1 right) like new Higgs bosons, R-parity violating scalar neutrinos, or new heavy vector bosons, etc.

Since the discovery of the muon and the realization that the muon is the electron's *big brother*, the origin of flavor stems as one of the outstanding puzzles in elementary particle

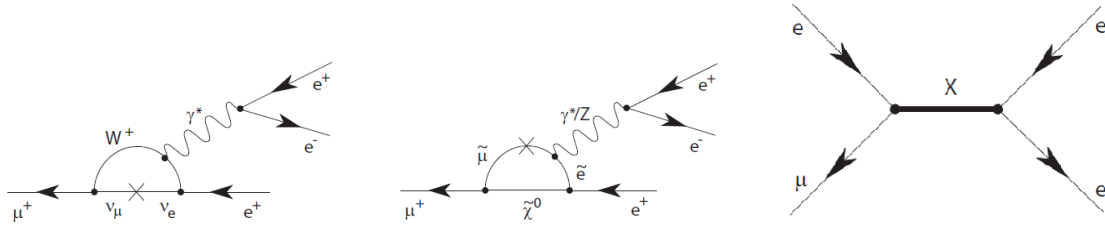


Figure 1: (left to right) Standard Model Feynman diagram for the neutrinoless $\mu^+ \rightarrow e^+ e^+ e^-$ process via neutrino mixing, diagram for cLFV involving supersymmetric particles (dipole type interaction), diagram for cLFV at tree level involving new particles (contact type interaction).

33 physics. Figure 3 summarizes the searches for cLFV performed by various experiments
 34 starting back in the 50's. Since none of the experiments has observed any of these processes,
 35 new upper bounds on cLFV processes have been set. Figure 3 also includes sensitivity
 36 projections for the next generation of cLFV experiments, which are about to start taking
 37 data.

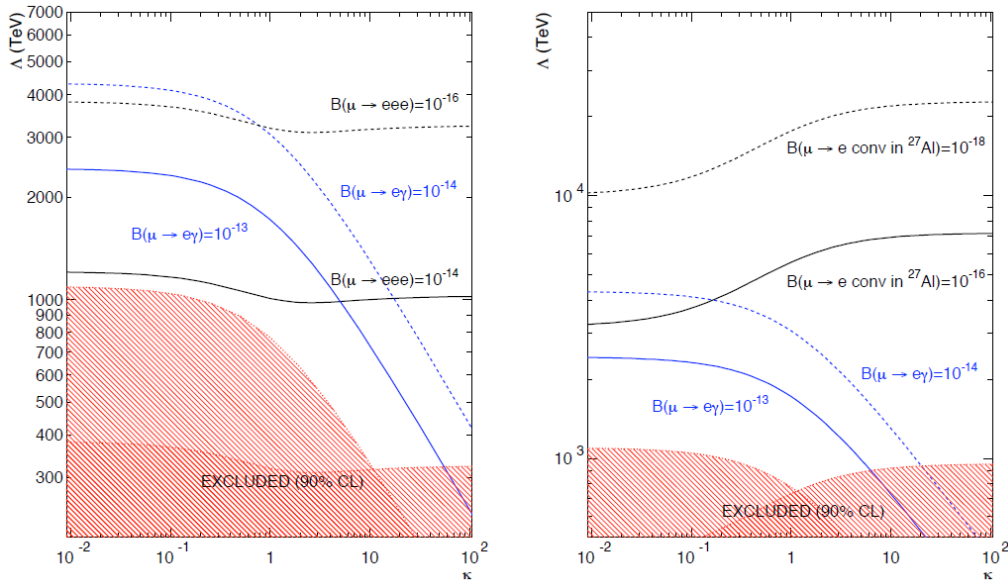


Figure 2: Reach for new physics in terms of an effective mass scale Λ in $\mu \rightarrow e\gamma$ and $\mu \rightarrow eee$ decays (left) and $\mu \rightarrow e$ conversions (right) [1] for different experimental sensitivities. κ is a parameter that weights the relative strength of dipole type contributions to four-fermion contact interactions and strictly speaking only $\kappa = 0$ (dipole int.) and $\kappa \rightarrow \infty$ (contact int.) are of interest, since it is very unlikely that different mechanisms will contribute at similar scales. The reach of the $\mu \rightarrow eee$ decay (left) for dipole type interactions ($\kappa \rightarrow 0$) could be significantly increased, if the process is mediated by the exchange of a Z boson instead of a photon.

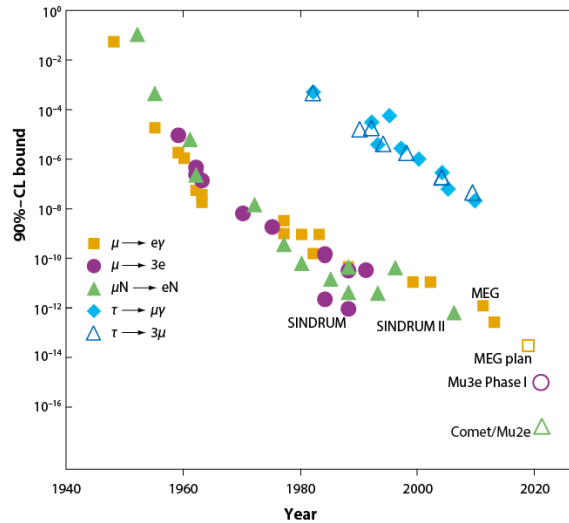


Figure 3: History of cLFV searches: evolution of upper bounds (90% C.L.) for cLFV processes set by various experiments over more than 60 years. The figure includes also sensitivity projections for the next generation of cLFV experiments, which are about to start taking data (Figure adapted from [3]).

38 2 The Mu3e Experiment

39 A new experiment to search for the cLFV neutrinoless muon $\mu^+ \rightarrow e^+e^+e^-$ decay is in
 40 preparation at the Paul Scherrer Institute [4] using the world’s most intense continuous
 41 muon beamline. With a projected sensitivity of 10^{-16} (90% C.L. in the absence of a
 42 signal), Mu3e has the potential of probing new physics at the PeV scale (see Figure 2).
 43 This represents a four orders of magnitude improvement w.r.t. previous searches performed
 44 at PSI by the SINDRUM experiment [5] ($BR \leq 2.4 \times 10^{-12}$ at 90% C.L.). The cLFV decay
 45 $\mu^+ \rightarrow e^+e^-e^+$ is complementary to the $\mu^+ \rightarrow e^+\gamma$ decay and $\mu^-A \rightarrow e^-A$ conversion,
 46 since it probes different mechanisms for cLFV. It is also complementary to direct searches
 47 of Beyond the SM physics at the LHC.

48 Reaching this sensitivity requires:

- 49 (i) a detector with a large geometrical acceptance,
- 50 (ii) the ability to measure around 10^{17} μ^+ decays over the lifetime of the experiment,
- 51 (iii) the ability to suppress any possible background (from physics, accidentals, and rein-
 52 teractions) to a level below 10^{-16} , and
- 53 (iv) a very high intensity continuous muon beam of $10^8 - 10^9$ stopped muons per second.

54 Experimentally the $\mu^+ \rightarrow e^+e^+e^-$ decay is identified by measuring two positrons and
 55 one electron originating from a common vertex in space and same time. In the Mu3e
 56 experiment the μ^+ ’s are stopped and decay at rest. Therefore, the energies of the electron
 57 and positrons sum up to the muon mass, whereas the sum of their momenta vanishes. Any
 58 other process that mimics this signature is a potential source of background and must be
 59 suppressed below the sensitivity level.

60 The first phase (phase I) of the experiment has been already approved and the construc-
 61 tion of the detector has recently started after an intense R&D program. In phase I the sen-
 62 sitivity goal is set at $BR(\mu^+ \rightarrow e^+e^+e^-) \leq 2 \times 10^{-15}$. This sensitivity can be achieved with
 63 a muon beam intensity of 10^8 μ^+ per second, which can be provided already now by the
 64 existing PSI muon beamline. Reaching the sensitivity goal of $BR(\mu^+ \rightarrow e^+e^+e^-) \leq 10^{-16}$
 65 will require a muon stopping rate of 2×10^9 μ^+ per second or higher.

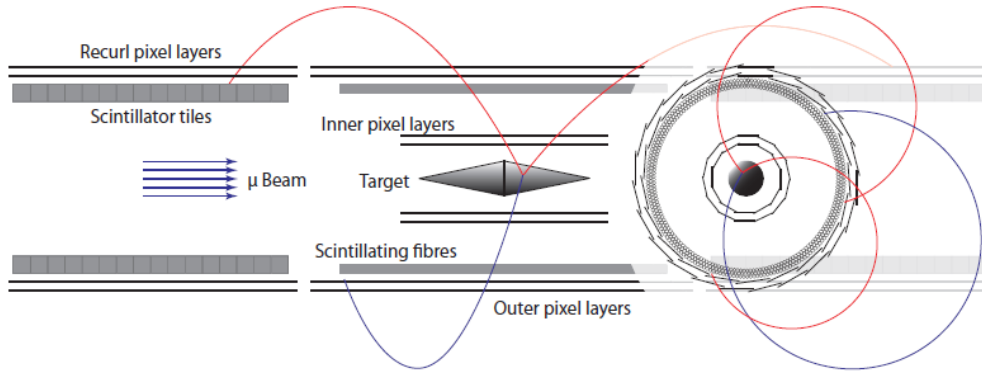


Figure 4: Schematic view of the Mu3e detector in phase I configuration (side view and cross section) showing all detector's components: the target, the inner silicon pixels, the scintillating fiber tracker, and the outer silicon pixels in the central region, and the scintillating tiles and the silicon pixels in the recurl stations. Two additional recurl stations will be added in phase II. The total length of the full detector is around 180 cm and the diameter is about 15 cm. The detector is inserted into a 100 cm diameter and 300 cm long superconducting solenoid providing a uniform magnetic field of 1 T.

66 2.1 The Muon Beam

67 The Paul Scherrer Institute (PSI) hosts the world's most intense proton beam of 590 MeV/c.
 68 The continuous surface muon beam is produced by extracting muons from the decay of
 69 pions, that were produced by impinging the proton beam on a carbon target and that
 70 decayed close to the target surface. Mu3e will be located at the $\pi E5$ beamline, which
 71 extracts and transport surface muons of 28 MeV/c. The same beamline is also used by
 72 the MEGII experiment. The compact muon beam line (CMBL), that is already installed
 73 in the experimental area of Mu3e, allows to easily switch between one experiment and
 74 the other (they will be operated alternately). It has already been demonstrated that the
 75 CMBL can provide rates of $10^8 \mu/s$. A new high intensity muon beamline HiMB is cur-
 76 rently under investigation at PSI, with the aim to provide even higher muon beam rates.
 77 This would enable Mu3e to reach the final sensitivity goal in phase II.

78 2.2 Detector Design

79 The Mu3e detector geometry is optimized to reach the highest possible momentum res-
 80 olution in a multiple Coulomb scattering environment, which is needed to suppress the
 81 dominating background from the $\mu^+ \rightarrow e^+ e^+ e^- \bar{\nu}_\mu \nu_e$ radiative decays. Minimizing the
 82 material within the acceptance of the detector is crucial to achieve these goals. Another
 83 source of background arises from the accidental combination of any two positrons and
 84 an electron that within the detector resolution shows the characteristics of the decay
 85 signal. As an example, this could be a positron from the dominant muon Michel decay
 86 $\mu^+ \rightarrow e^+ \bar{\nu}_\mu \nu_e$ in combination with a positron and electron from a Bhabha scattering event
 87 or photon conversion. The rate of the accidental background grows quadratically with
 88 beam intensity and can be suppressed by precise time and vertex resolution in addition to
 89 momentum resolution.

90 The momentum is measured via the bending radius of the particles in a magnetic
 91 field. Hence, the momentum resolution improves with the lever arm between two position
 92 measurements. The optimum momentum resolution is achieved after about a half turn,
 93 because at this point uncertainties caused by multiple scattering cancel to first order. For
 94 this reason, the Mu3e experiment relies on measuring recurling tracks. When a particle

95 has passed the outer detector layer, it will not cross further material and following a helical
 96 trajectory it will eventually hit the outer layers again. Between those two measurements,
 97 it has performed about a half turn.

98 The key elements of the Mu3e detector are illustrated in Figure 4:

99 (i) a high precision tracker based on HV-MAPS [6], providing high spatial resolution, and
 100 (ii) a time-of-flight (ToF) system, consisting of scintillating fibers in the central region
 101 coupled to silicon photomultipliers arrays [7] and scintillating tiles also coupled to Si-PMs
 102 in the outer regions, providing very precise timing information at very high particle rates.

103 By combining both detector technologies all backgrounds can be reduced below the
 104 aimed sensitivity of $BR(\mu^+ \rightarrow e^+e^+e^-) \sim 10^{-15}$ (see Figure 11). All elements are placed
 105 in a 300 cm long homogeneous solenoidal magnetic field of 1 Tesla. Surface muons of 28
 106 MeV/c produced by the PSI beamline are stopped on a hollow double cone aluminum
 107 target. The design of the target maximizes the surface where muons stop and decay in
 108 order to maximize the separation of the decay vertexes.

109 The Mu3e tracking detector is designed such to be sensitive for a transverse momentum
 110 range from 10 to 53 MeV/c (Figure 5 (left) shows the fractional coverage of the $\mu \rightarrow eee$
 111 decay as a function of the lowest detectable positron energy) and to provide a momentum
 112 resolution better than 0.5 MeV/c over the same range, in order to suppress the $\mu^+ \rightarrow$
 113 $e^+e^+e^- \bar{\nu}_\mu \nu_e$ radiative decays, as shown in Figure 5 (right). This kinematical coverage
 114 corresponds to an acceptances of 50% or more for all considered cLFV models.

115 3 The Pixel Tracking Detector

116 Electrons from muon decays are detected by two cylindrical double layer silicon pixel de-
 117 tectors, one double layer just above the target, which allows for a precise determination
 118 of the decay vertex, and the second at a 7.5 cm radius, enabling the momentum mea-
 119 surement. Curling tracks are measured by a second cylindrical double layer silicon pixel
 120 detector, also at the same 7.5 cm radius, upstream and downstream of the central detector,
 121 for a total of at least 6 measured space points per track. By also measuring the curling
 122 part of the track one achieves a large lever arm.

123 The technology adopted for the Mu3e pixel detectors is based on the high-voltage

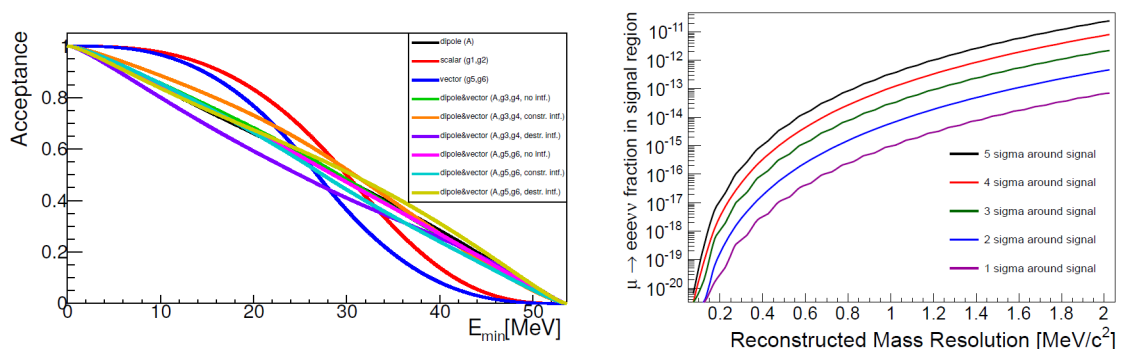


Figure 5: Coverage of the $\mu \rightarrow eee$ decay as a function of the lowest detectable positron energy for different effective cLFV models. The black line corresponds to pure dipole and the red and blue lines to pure four-fermion contact interaction models whereas the other lines correspond to a mixture of dipole and vector interactions (left). Contamination of the signal region (one sided cut) with internal conversion events ($\mu \rightarrow eee \nu \bar{\nu}$) as a function of the visible three-particle mass resolution (right).

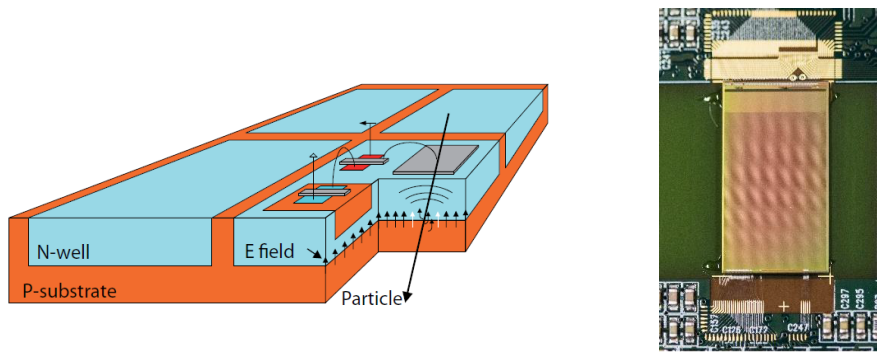


Figure 6: Schematic of a pixel sensor in HV-MAPS technology [6] (left) and photo of the MuPix8 sensor prototype with an active area of $19 \times 10 \text{ mm}^2$ (right).

124 monolithic active pixel sensors (HV-MAPS) in CMOS technology [6] (see Figure 6). The
 125 individual pixels are implemented as deep N-wells in a p-doped substrate and are reversely
 126 biased to around 80 V. Ionization charges generated by traversing particles are quickly
 127 collected within $\mathcal{O} \sim 1 \text{ ns}$. The charge collection is limited to a thin depleted zone of 10 to
 128 $20 \mu\text{m}$ close to the sensor surface. Therefore, the sensors can be thinned down to $50 \mu\text{m}$
 129 providing a very lightweight detector. Moreover it is possible to implement transistors
 130 within the pixel and thus build analog and digital logic directly on the HV-MAPS sensor
 131 itself allowing for amplification and digitization of the signals already on the chip with no
 132 additional electronics. Signal amplification and shaping is performed in the pixel itself,
 133 whereas the digitization takes place in the periphery, a small part at the bottom edge of the
 134 sensor. The sensor has digital, zero-suppressed data output with a fast serial link of
 135 1.25 Gbit/s . A pixel size of $80 \times 80 \mu\text{m}^2$ is planned for the final sensor with an active area
 136 of $2 \times 2 \text{ cm}^2$ per sensor. The development of the sensors is in the final prototyping stage.
 137 With a pixel size of $80 \times 80 \mu\text{m}^2$ the HV-MAPS tracker will consists of 180 million pixels
 138 (phase I).

139 Figure 7 illustrates the performance of the MuPix8 sensor prototype with an active
 140 area of $2 \times 1 \text{ cm}^2$ and a pixel size of $80 \times 81 \mu\text{m}^2$ (very close to the final design). This
 141 prototype has been thinned down to $60 \mu\text{m}$. The sensor has been extensively tested,
 142 yielding efficiencies in excess of 99% with very low noise, little cross-talk, and few dead
 143 pixels. In order to improve the timing resolution, the MuPix8 incorporates also signal
 144 amplitude measurements allowing to correct for time-walk. A time resolution of around
 145 14 ns has been achieved after time-walk corrections.

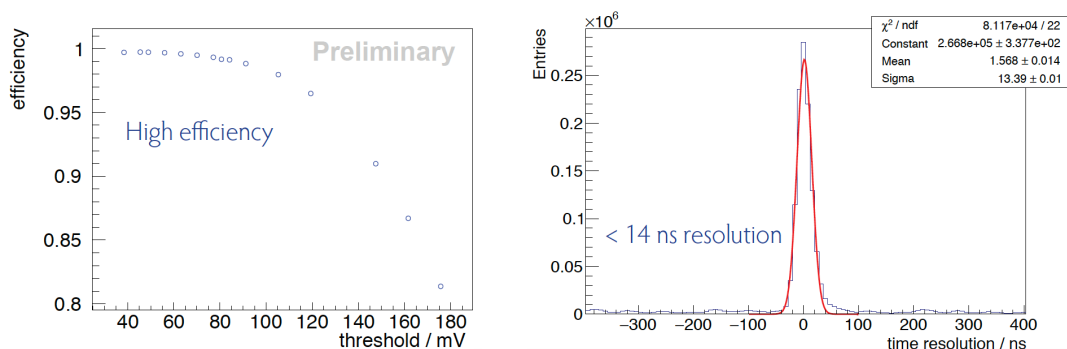


Figure 7: Performance of the MuPix8 pixel sensor prototype: efficiency (left) and time resolution (right) obtained in testbeam measurements.

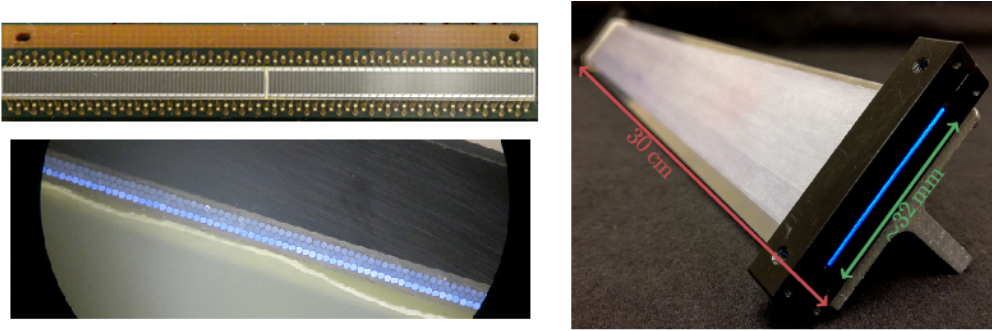


Figure 8: 128 ch. Si-PM array used for the readout of scintillating fibers (top left), microscope photo of a three layer staggered SciFi ribbon profile (bottom left), and SciFi ribbon prototype close to the final size (right).

146 4 The Timing Detectors

147 The combinatorial backgrounds can be efficiently suppressed by timing measurements.
 148 For this purpose, the silicon tracker is complemented by a cylindrical time of flight (ToF)
 149 detector consisting of a very thin scintillating fiber tracker in the central region and scintil-
 150 lating tiles in the recurl stations. The scintillating fiber detector (SciFi) is placed directly
 151 below the outer pixel layers. The main role of the ToF system is to measure very precisely
 152 the time of production of various particles in order to reject pile-up events (accidental
 153 backgrounds) with very high efficiency. With the combination of timing information from
 154 the fiber and tile detectors, background suppression factors of about 100 with two corre-
 155 lated and one uncorrelated track can be achieved. Backgrounds with three uncorrelated
 156 tracks are even more strongly suppressed. In addition, the SciFi detector will help to
 157 determine the charge of the recurling tracks in the central region of the apparatus by
 158 determining the sense of rotation for charged tracks.

159 Figure 8 shows the components of the SciFi detector. The SciFi arrays are formed by
 160 staggering 3 layers of double clad 250 μm diameter scintillating fibers (Figure 8 bottom
 161 left), for an overall thickness smaller than 0.2% of a radiation length. The SciFi tracker
 162 consists of 12 ribbons (Figure 8 right), 30 cm long and 32 mm wide. The ribbons are
 163 arranged cylindrically at a 6 cm radius. The fibers are read out at both end with 128
 164 channel Si-PM arrays (Figure 8 top left). By arranging the individual cells of the Si-PM
 165 into columns one obtains a sensor consisting of 250 μm wide independent readout channels
 166 with a common cathode.

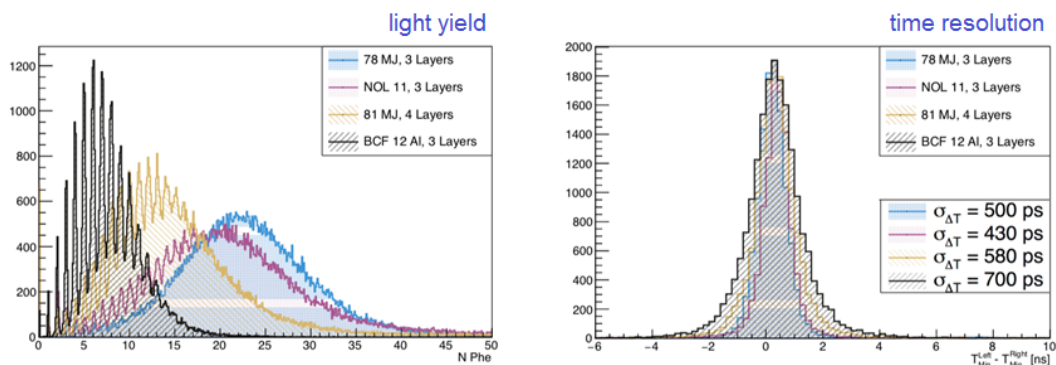


Figure 9: Characterization of different scintillating fibers: light yield (left) and measured time resolution (right).

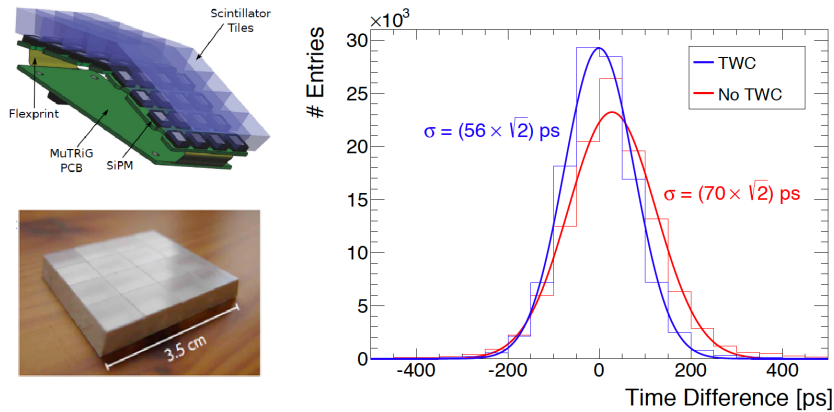


Figure 10: Overview of the scintillating tile detector in the recurling stations of the Mu3e apparatus: design of the detector (top left), the scintillating tile matrix (bottom left), and achieved time resolution (right).

167 Different scintillating materials have also been evaluated, as shown in Figure 9 left.
 168 In testbeam studies an efficiency in excess of 96% with a spatial resolution of around
 169 $80 \mu\text{m}$ have been achieved for the three layer SciFi detector. Figure 9 (right) shows the
 170 time difference measured from both fiber ends for crossing particles. The crossing time is
 171 obtained by taking the meantime of both time measurements resulting in a time resolution
 172 two times better than for the time difference (i.e. half of the value reported in Figure 9).
 173 The best timing so far achieved is of 200 ps.

174 The curling tracks are measured a second time in the recurl stations. Figure 10 left
 175 illustrates the design of the scintillating tile detector, which consists of $8 \times 8 \times 8 \text{ mm}^3$
 176 scintillating cubes coupled individually to $3 \times 3 \text{ mm}^2$ Si-PMs. Figure 10 right shows
 177 the time resolution obtained for this detector. With time walk corrections a resolution
 178 better than 60 ps can be achieved. The SciFi arrays and the tiles are read out with a
 179 dedicated mixed mode ASIC, the MuTRiG, capable of sustaining rates in excess of a MHz
 180 per readout channel.

181 5 Mu3e Sensitivity

182 The final sensitivity of the Mu3e experiment depends on the ability to reduce acciden-
 183 tal backgrounds, and irreducible backgrounds (physics) such as the $\mu^+ \rightarrow e^+e^+e^- \bar{\nu}_\mu \nu_e$
 184 radiative decays. In addition, one has to also identify and reject reinteractions in the de-
 185 tector materials. Accidental backgrounds can be efficiently suppressed by excellent timing
 186 (few 100 ps) and vertex resolution. The suppression of physics backgrounds requires high
 187 momentum resolution ($\sigma_E < 0.5 \text{ MeV}$) in order to reconstruct precisely the μ^+ decay
 188 kinematics. The following criteria will be exploited:

- 189 (i) energy and momentum conservation (all 3 outgoing electrons are coplanar with zero
 190 total momentum and the total energy reproduces the parent muon mass),
- 191 (ii) vertex reconstruction (all 3 tracks originate from the same point), and
- 192 (iii) timing (all 3 tracks are produced in a very narrow time window).

193 Figure 11 illustrates the ability of the proposed Mu3e detector to separate the $\mu^+ \rightarrow$
 194 $e^+e^+e^-$ signal at different branching ratios from the radiative decay with internal conver-
 195 sion and accidental combinations of electrons from Bhabha scattering and Michel decays.
 196 The detector performs well enough to separate signal $\mu^+ \rightarrow e^+e^+e^-$ decays from back-
 197 ground even at a branching ratio of 10^{-15} .

